INTERNATIONAL JOURNAL FOR NUMERICAL AND ANALYTICAL METHODS IN GEOMECHANICS
Int. J. Numer. Anal. Meth. Geomech. 2009; **33**:1867–1888
Published online 22 April 2009 in Wiley InterScience (www.interscience.wiley.com). DOI: 10.1002/nag.796

Effect of the water/cement ratio on concrete behavior under extreme loading

Xuan Hong Vu[1], Yann Malecot[1,*,†], Laurent Daudeville[1] and Eric Buzaud[2]

[1]*Université Joseph Fourier – Grenoble I, Laboratoire 3S-R, CNRS, INPG, BP53, 38041 Grenoble Cedex, France*
[2]*DGA, Centre d'Etudes de Gramat, 46500 Gramat, France*

SUMMARY

This study focuses on identifying concrete behavior under severe triaxial loadings (near field detonation or ballistic impacts). In order to reproduce high stress levels with well-controlled loading paths, static tests have been carried out on concrete samples by mean of a very high-capacity triaxial press (stress levels on the order of 1 GPa). It is a longstanding fact that the water/cement ratio (W/C), upon entering the concrete composition, is a major parameter affecting the porosity and strength of the cement matrix of hardened concrete. The objective of this article is to quantify the effect of this ratio on concrete behavior under conditions of high confinement. From the composition of a reference 'ordinary' concrete (i.e. W/C = 0.6), two other concretes have been produced with W/C ratios equal to 0.4 and 0.8, respectively. This article presents experimental results and their analysis regarding the effect of water/cement ratio (W/C) on concrete behavior under high confinement. It shows that when placed under high confinement, concrete behaves like a granular stacking composed of concrete without any influence from the level of cement matrix strength. Copyright © 2009 John Wiley & Sons, Ltd.

Received 9 October 2008; Revised 5 March 2009; Accepted 9 March 2009

KEY WORDS: concrete; water/cement ratio; triaxial test; high confinement; criterion; experiment

1. INTRODUCTION

This study focuses on identifying concrete behavior under extreme loading situations (near field detonation or ballistic impacts, etc.). During such loadings, the concrete is subjected to very high-intensity triaxial stress states. Upon impact of a rigid projectile on a massive concrete structure, three triaxial behavior phases can be observed. Each phase is associated with different damage modes, which may sometimes occur simultaneously [1, 2]. On the face nearest to the structure,

*Correspondence to: Yann Malecot, Laboratoire 3SR, Domaine Universitaire, BP53, 38041 Grenoble cedex 9, France.
†E-mail: yann.malecot@ujf-grenoble.fr, yann.malecot@hmg.inpg.fr

Contract/grant sponsor: 'Centre d'Etudes de Gramat' (CEG, DGA)

spalling is detected, which from a mechanical perspective can be associated with unconfined tension. Penetration of the projectile into the structural core is the source of a triaxial compression, while inertia of the structure creates a passive confinement within the zone located around the projectile. Moreover, if the target is thin enough, during the final penetration phase, simple tension and shear stresses on the distal face of the concrete are observed. In extreme cases, the impact may end with a full perforation of the target. The validation of concrete behavior models, which simultaneously take into account the phenomena of brittle damage and irreversible strain such as compaction, thus requires test results that enable reproducing the complex loading paths described previously.

Most of the experimental results available in the literature only pertain to triaxial loadings with a moderate level of confining pressure [3–9]. In particular, these authors have revealed the transition from brittle to ductile behavior that characterizes cohesive materials. Numerous studies have shown that dynamic tests on concrete, e.g. using split Hopkinson pressure bars [10, 11], are difficult to perform, due primarily to the brittle nature of the material, which then leads to rupture during the transient loading stage. The inhomogeneous characteristic of the stress state in the sample, along with the very limited control over the loading path and relatively poor instrumentation, complicate test result interpretation. However, the test results available in the literature show the resistance of concrete to be an increasing function of the rate of loading. This dependence of the concrete behavior on the rate of loading seems to be quite limited in the absence of a liquid phase [12, 13]. It is however much higher on traction and can be explained in great part by the influence of defects [14]. It has also been shown that rate effects in dynamic uniaxial tensile loading are much higher for wet samples than for dried ones [15]. The dynamic triaxial behavior of the concrete is a little studied domain. Confined Hopkinson bars tests have been investigated by Schmidt on concrete samples up to 7 MPa confining pressures. These tests show a decrease in the sensitivity of the concrete response to the rate of loading when the confinement increases [16].

Higher rates of loadings can be achieved by mean of the plate impact technique. This type of experiment allows to identify the material equation of state (i.e. pressure - volume relation) at stress levels of several GPa.

The results presented in this article make reference to static triaxial tests carried out on concrete samples by mean of a high-capacity hydraulic triaxial press, called the 'GIGA' press. This experimental device makes it possible to reach, within the samples, stress levels on the order of 1 GPa with static, homogeneous and well-controlled load paths.

Deriving the static characterization of a constitutive model in order to predict dynamic behavior is not a new practice in the study of geomaterials. Previous experimental studies have been essentially limited to small mortar samples [17–20]. Such studies emphasize the increase in maximum deviatoric stress of the mortar and the evolution in mortar limit states with confinement. The aim of the present study is to extend this practice to the study of 'actual' concrete materials (i.e. with an aggregate dimension on the order of a centimeter).

The comparative study between a concrete and a mortar with a confining pressure of 500 MPa, as conducted by S. Akers and Phillips [21], highlights the differences in behavior between two materials and moreover shows that the study of mortar behavior under high confinement is not representative of concrete behavior. Other triaxial test results on ordinary concrete with confining pressures ranging between 0 and 500 MPa yield the evolution in behavior and limit state of the concrete with confinement [22, 23].

Since 2004, the laboratory 3S-R has launched in collaboration with the 'Centre d'Etudes de Gramat' ('Délégation Générale pour l'Armement' (DGA), French Ministry of Defense) a research program on the vulnerability of concrete infrastructures. In a previous stage of this program,

DOI: 10.1002/nag

using the same baseline material, Gabet studied the influence of loading path on the concrete behavior [24], Poinard studied the influence of the confinement on the cracking pattern [25] and Dupray realized a mesoscopic model of these experiments [26]. In particular, these results indicated that under high confinement, the limit state of the concrete remains relatively independent of both the loading path and Lode's angle. Using the same baseline material, the effect of the saturation ratio on the concrete behavior under high confinement has been studied too [27]. The mentioned study shows that the saturation ratio exerts a major influence on concrete behavior, particularly on both the concrete strength capacity and shape of the limit state curve for saturation ratios above 50%. It also highlights that while the strength of dried concrete strongly increases with confining pressure, it remains constant over a given confining pressure range for either wet or saturated samples. During a latter stage of this research program, the strain rate effects on concrete behavior will be studied by means of both split Hopkinson pressure bar and plate impact tests conducted on concrete samples.

In this article, the focus lies more specifically with effects of the water/cement ratio (W/C), entering the fresh concrete composition, on hardened concrete behavior under very high confinement. The effect of W/C ratio on concrete strength in unconfined compression is already quite well known. According to the rules governing the calculation of concrete structures, concrete is essentially characterized by its strength in unconfined compression after 28 days of ageing, f_{c28}. Based on empirical relations, the majority of the other characteristics can then be deduced from f_{c28} (tensile strength, Young's modulus, etc.).

For a given type of aggregate and cement however, f_{c28} depends almost exclusively on either the cement paste composition or W/C ratio [28–33]. The W/C ratio also influences the porosity of the cement matrix within the hardened concrete [34–36], which itself heavily influences concrete durability [37]. The dependence of concrete triaxial behavior on W/C ratio is thus a major factor to the present study. Confined uniaxial tests carried out at high stress levels on mortars for various W/C ratios reveal that material compaction is correlated with its internal porosity [19, 38]. Mortar compaction thus increases with W/C ratio. Triaxial compression tests performed at low confinement levels (less than 15 MPa) have moreover highlighted that the deviatoric stress, Young's modulus and compressibility modulus of the mortar also decrease as the W/C ratio increases [39]. On the other hand, no results have yet been produced on the effect of W/C ratio with respect to the triaxial behavior of concrete under high confinement.

The experimental device used in this study will be described in the following section. Results from the triaxial tests carried out on three concrete materials featuring different W/C ratios will then be presented, first in terms of stress–strain curves (Section 3), then in terms of volumetric and deviatoric behavior curves (Section 4), and subsequently in terms of limit state curves (Section 5). These results show that contrary to what has been observed in unconfined compression and at low confining pressures, the deviatoric behavior of the concrete materials becomes insensitive to W/C ratio at high confinement levels.

2. EXPERIMENTAL SET-UP

2.1. Triaxial cell

A high-capacity triaxial press has been especially designed for this study [40]. The development of a test procedure on concrete that has proven to be rather complex is presented in detail in the

DOI: 10.1002/nag

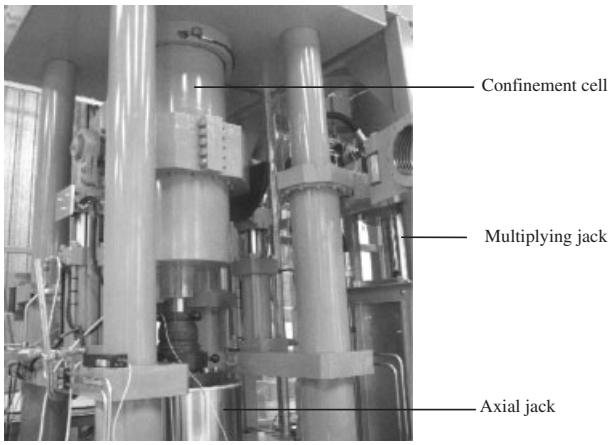

Figure 1. General view of the GIGA press.

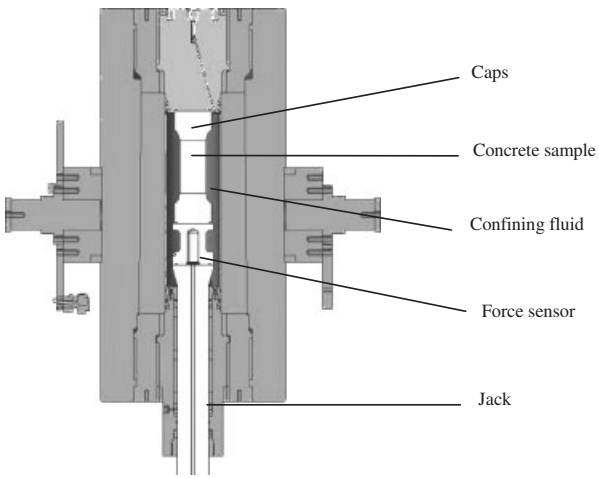

Figure 2. Cross-section view of the confining cell.

Ph.D. Thesis of X. H. Vu [41]. Figure 1 provides an overview of the 'GIGA' press. A cross-section of the confining cell is shown in Figure 2. This press is able to generate a confining pressure of up to 0.85 GPa and an axial stress reaching 2.3 GPa on a cylindrical concrete specimen 7 cm in diameter and 14 cm long (Figure 3).

The concrete sample is placed inside the confining cell while the confining fluid, a di-2-ethylhexyl azelate (DOZ), which contains a non-volatile, inert and highly incompressible organic component, gets injected into the cell through the upper opening. This fluid is then pressurized by means of a system of multiplying jacks. The axial force is generated from a 13 MN jack located underneath the cell and then transmitted to the sample by a piston passing through the lower plug of the confining cell. An axial displacement sensor located in the press is used to control axial jack displacement,

DOI: 10.1002/nag

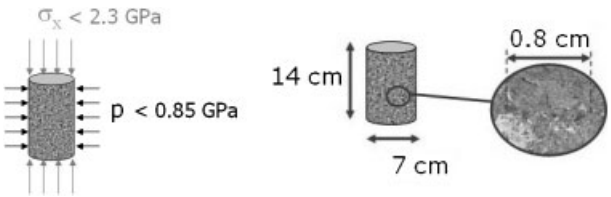

Figure 3. Maximum press capacity and associated sample sizes of the triaxial cell.

whereas an axial load sensor and pressure sensor placed inside the confining cell display the stress state of the sample. The confining pressure and axial jack displacement are servo-controlled, which offers several possible loading paths.

2.2. *Strain measurements*

Strain measurements are performed by means of an axial sensor LVDT, along with one axial and two circumferential gauges (see Figure 4). The gauges used for this study, EP-08-10CBE-12 type from Vishay Micro-measurements Company, are 28 mm long, i.e. about three times the size of the largest aggregate. These gauges allow strain measurements up to 15%. The LVDT sensor used for this study, 500XS-3013 type from Schaevitz Sensors Company, consists of a transformer and of a movable magnetic core. Each part of the LVDT sensor is fixed on a loading head. It permits to measure a relative displacement up to 50 mm.

The axial gauge yields a local measurement whereas the LVDT gives a global measurement of the axial strain. The comparison between these two measurements allows a rough evaluation of the sample strain homogeneity. The circumferential strain is measured by means of two diametrically opposite gauges, such that the probability of maintaining a measurement until the end of the test increases. These two gauges also allow another control of the strain homogeneity. The use of gauges on concrete for triaxial compression tests in the presence of such high confinement levels is, to the best of our knowledge, unprecedented.

2.3. *Characteristics of concrete samples*

Sample protection. Given the porous nature of concrete, the high level of confinement has required the development of a multilayer protective membrane around the sample; this element is composed of 8 mm of latex and 2 mm of neoprene (see Figure 5). This setup prevents the confining fluid from penetrating inside the sample. In addition, a plastic shield placed on the gauges protects them against possible puncture of the membrane [42]. Figure 5 shows the shield as well as the membrane, set up sequentially around the sample.

Concrete composition. In order to study the effect of W/C ratio on concrete behavior, three concretes with different W/C ratios were produced. The composition of the reference concrete, for which an exhaustive experimental study was carried out [24, 41], is provided in the EC06 column of Table I. This mix design corresponds to an ordinary concrete in terms of both the strength and the slump. It can however be noted that the very high quality cement used, for purposes of better controlling material reproducibility, leads to a particularly low cement volume. Aggregates compound 99% quartzite are derived from natural deposit (rolled aggregates, 99% quartzite). Its maximal size (8 mm) was selected by taking the sample diameter (70 mm) into account.

DOI: 10.1002/nag

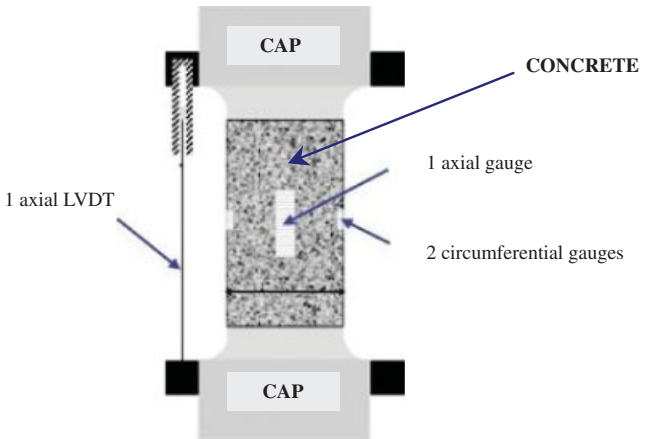

Figure 4. Schematic diagram of the strain measurement procedure conducted on the sample.

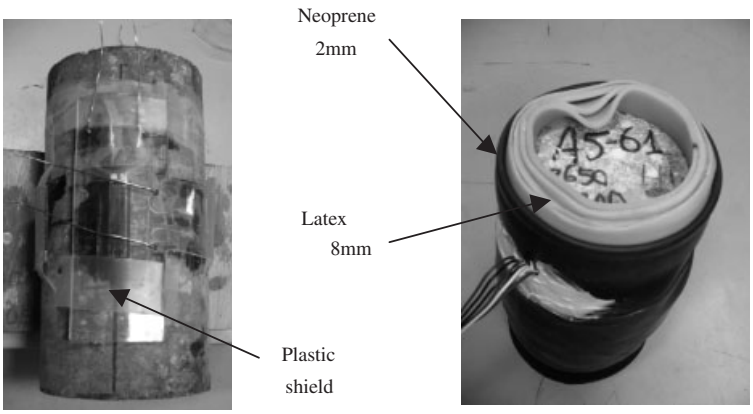

Figure 5. Protective device placed around the sample: Plastic shield (left photograph) and multilayer membrane (right).

Based on the composition of this reference concrete (labeled EC06), whose W/C ratio equals 0.64, two modified concretes with W/C ratios, respectively, equal to 0.4 (concrete EC04) and 0.8 (EC08) were produced. These two modified concretes contain a granular skeleton and cement paste volume very similar to those of the reference concrete (see Table I). Since a limited quantity of water was used for concrete EC04, the 'Sikafluid' superplasticizer has been added in order to yield a slump of 7 cm, i.e. equivalent to that of concrete EC06. Concrete EC08, on the other hand, has a 14 cm slump, clearly higher than that of the other two concretes.

Sample making. A manufacturing procedure for the concrete samples was established with the aim of ensuring minimal variability of the mechanical properties of concrete. All concretes were cast within a parallelepiped mould by batches 13.5 l in volume. The placement of concretes EC06

DOI: 10.1002/nag

Table I. Compositions and mechanical properties of concretes EC04, EC06, EC08.

	EC04	EC06	EC08
Concrete composition			
0.5/8 'D' gravel (kg/m^3)	1000	1008	991
1,800 µm 'D' sand (kg/m^3)	832	838	824
CEM I 52.5 N PM ES CP2 cement (Vicat) (kg/m^3)	349	263	226
Water (kg/m^3)	136	169	181
Sikafluid Superplasticizer (kg/m^3)	4.5	0	
Volume of occluded air in fresh concrete (l/m^3)	41	34	50.5
Density (kg/m^3)	2322	2278	2252
W/C ratio	0.39	0.64	0.80
Cement paste volume V_p (m^3/m^3)	0.250	0.252	0.248
Concrete properties			
Unconfined compressive strength after 28 days of ageing (MPa)	57*	28.6	21*
Average slump measured using the Abrams cone (cm)	7	6.9	14
Porosity accessible to water (%)	7	12	14

*Estimated values based on unconfined compression tests conducted after 28 days of ageing.

and EC04, which display identical slumps, was carried out by vibration on a vibrating table for a 30-second period. In contrast, the placement of concrete EC08 was carried out by simple pricking.

The concrete block, removed from the mould 24 h after casting, is conserved for 28 days in a saturated environment within plastic bags immersed in water in order to insulate the concrete both physically and thermally. The block is then cored, cut and ground. All these machining stages are carried out under water lubrication to avoid heating the concrete. The defect in parallelism of the two sample faces is less than 0.1 mm for a 70-mm diameter.

Sample conservation. After machining, the samples were conserved in water for 3 months, in accordance with an identical conservation procedure for all concretes. The samples were then dried in a drying oven at 50°C temperature and 8% relative humidity. All samples tested in this study were conserved in the drying oven for a period of between 3 and 6 months. It should be noted that after 1 month of drying in the oven, the daily variation in relative sample mass does not exceed 0.1%, the sample mass can be considered as stabilized.

We studied the evolution in strength for simple compression of the samples vs drying time in the oven for three tested concretes. Findings prove that the variation in strength between samples conserved in the drying oven for 3 months or 6 months is less than 12%; this variation figure is just slightly higher than the 7% dispersion in results measured on concrete EC06 samples of an identical age. For the remainder of this article, the concrete age effect on triaxial test results will thus be neglected; it will be considered that the results are characteristic of an 8-month-old concrete, conserved 4 months in water at 20°C then another 4 months in a drying oven at 50°C.

2.4. Loading path

Except for the unconfined compression tests, all triaxial compression tests have been carried out using a similar loading path of the triaxial compression type. The test begins with a hydrostatic phase, during which confining pressure increases at a rate of 1.67 MPa/s until reaching the desired

DOI: 10.1002/nag

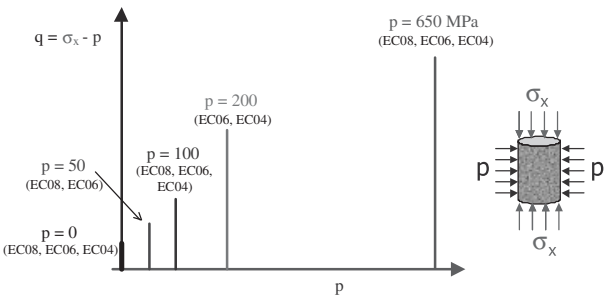

Figure 6. Loading path of the completed tests: deviatoric stress q vs confining pressure p; σ_x: axial stress; EC08: W/C = 0.8; EC06: W/C = 0.64; EC04: W/C = 0.4.

pressure. The deviatoric phase is then conducted, at constant confining pressure, by imposing a constant displacement rate of 20 μm/s for the axial jack. This rate corresponds to a strain rate of approximately 10^{-4}/s for the sample. Note that the maximum deviatoric stress value is not imposed but is a result of the test. The unloading phase is symmetrical in comparison with the loading phase.

Figure 6 serves to summarize the loading paths of all tests carried out during this study.

It should be noted that stresses are counted as positive in compression. σ_x denotes axial stress, p the confining pressure, σ_m the mean stress, and q the scalar deviatoric stress, i.e.

$$\sigma_m = \frac{\sigma_x + 2p}{3} \tag{1}$$

$$q = \sigma_x - p \tag{2}$$

The unconfined compression tests were performed on a different press of the 3S-R Laboratory with a more adequate and accurate load sensor. These tests are controlled in displacement with a strain rate of approximately 10^{-5}/s. The samples feature the same dimensions as those used in the triaxial tests. A summary of the tests conducted appears in Table II.

3. TEST RESULTS

This section will display results from the unconfined compression tests, which serve to characterize and compare the uniaxial behavior of the three studied concretes. The results from triaxial compression tests will then be presented in terms of axial stress separately for the various strain components of each concrete.

3.1. Unconfined compression tests

Figure 7 shows results from the unconfined compression tests carried out on the three types of concrete. Figure 7(a) indicates the evolution in axial stress with respect to the strain components. As could be expected, an increase in Young's modulus E and ultimate stress $\sigma_{\max}$ of the concrete can be observed with a decrease in the W/C ratio. The numerical values of E, $\sigma_{\max}$ and Poisson's ratio obtained for the three concretes are listed in Table III. The elastic properties of each concrete are identified, by means of strain gages, in the linear range of the behavior ($0 < \sigma_x < 0.5\sigma_{\max}$). The low values of Poisson's ratio of concrete EC06 and EC08 are probably due to both to their

DOI: 10.1002/nag

Table II. Summary of tests conducted vs type of concrete and confining pressure.

Concrete	Confining pressure p (MPa)	Sample number
EC04 W/C = 0.39	0	EC04-3
	100	EC04-1
	200	EC04-4
	650 (n1)	EC04-5
	650 (n2)	EC04-8
EC06 W/C = 0.64	$p = 0$	A0-8
	50	A0-5
	100*	A9-75
	200*	A9-76
	650	A11-5
EC08 W/C = 0.80	0	EC08-4
	50	EC08-2
	100	EC08-9
	650	EC08-1

*Tests undertaken by Gabet *et al.* [24].

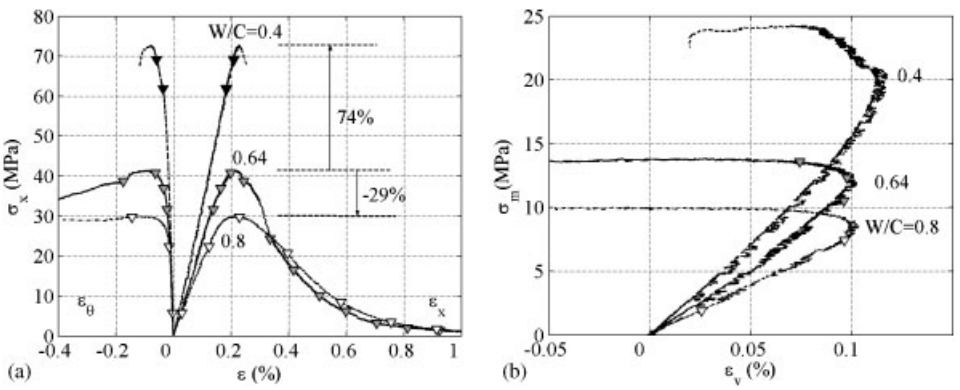

Figure 7. Unconfined compression tests: EC08 (white symbols), EC06 (gray symbols) and EC04 (black symbols): (a) axial stress σ_x vs strain components ε_x and ε_θ and (b) mean stress σ_m vs vol. strain ε_v.

low saturation ratio and to their high porosity level. In accordance with the literature [43, 44], it is noted that the increase in Young's modulus is proportionately lower than that of the concrete strength. Figure 7(b) also reveals that concrete EC04 has a brittle elastic type of behavior, while concretes EC06 and EC08 definitely show a more ductile behavior of the softening type. These results comply with expectations. Others uniaxial compression tests have been carried without any strain measurements [41]. The results show that the scatter of the ultimate stress is about 7%.

Figure 7(b) exhibits the evolution in mean stress vs the volumetric strain of concrete. During the test's contraction phase, for a given mean stress, it is observed that as the W/C ratio rises, volumetric strain drops. Since the granular skeleton of all three concretes is identically composed,

DOI: 10.1002/nag

Table III. Unconfined compression tests: Identification of the main concrete characteristics.

Concrete	EC08	EC06	EC04
W/C ratio	0.80	0.64	0.39
Ultimate stress σ_{max} (MPa)	30	42	73
Young's modulus E (GPa)	19	24	33
Poisson's ratio v	0.12	0.14	0.15

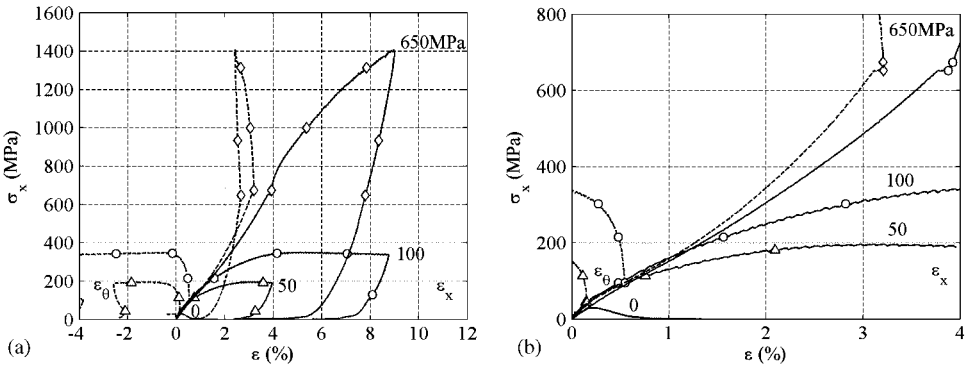

Figure 8. Triaxial tests conducted at different confining pressures p on concrete EC08 (W/C = 0.80): Axial stress σ_x vs strain components ε_x and ε_θ; $p = 0$ MPa (no marker); 50 MPa (triangle); 100 MPa (circle); 650 MPa (diamond); axial strain ε_x (full line); circumferential strain ε_θ (dash line). Zoom on the hydrostatic phases of the loading (figure on the right).

concrete porosity increases with W/C ratio. This result is also in perfect agreement with the evolution in Young's modulus and Poisson's ratio (Table III).

3.2. Triaxial tests

Figures 8–10 show the evolution in axial stress vs strain components for the triaxial compression tests with different confining pressures. Each graph corresponds to a given concrete composition. The scales on all three graphs are identical.

For a given concrete type, during the hydrostatic phase (Figures 8(b), 9(b) and 10(b)), it is observed that all the tests follow the same curve trend regardless of the confining pressure. This finding indicates good reproducibility of concrete behavior and confirms the relevance of the sample preparation procedure. In addition, during this phase, the axial and circumferential strain curves lie very close to each other. Concrete behavior therefore is nearly isotropic for these loading levels. For concretes EC06 and EC08 (Figures 9 and 8), it may be noted that stress–strain curves under hydrostatic loading reveal an '*s*' shape. After a rather short linear phase (up to 40–60 MPa of confinement), a tangential stiffness reduction of these concretes is seen to be followed by a subsequent stiffening from 200 to 300 MPa of confinement. The stiffness reduction can be attributed to the cement matrix damage beyond the elastic phase and stiffening with material densification as concrete pores close once the hydrostatic strain becomes significant. For concrete EC04 (Figure 10), a much longer linear phase can be detected (up to 200 MPa of confinement)

DOI: 10.1002/nag

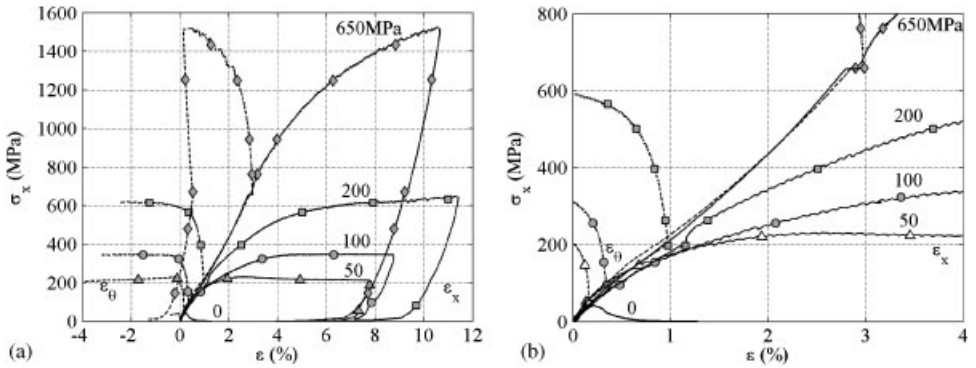

Figure 9. Triaxial tests conducted at different confining pressures p on concrete EC06 (W/C = 0.64): Axial stress σ_x vs strain components ε_x and ε_θ; $p = 0$ MPa (no marker); 50 MPa (triangle); 100 MPa (circle); 200 MPa (square); 650 MPa (diamond); axial strain ε_x (full line); circumferential strain ε_θ (dash line). Zoom on the hydrostatic phases of the loading (figure on the right).

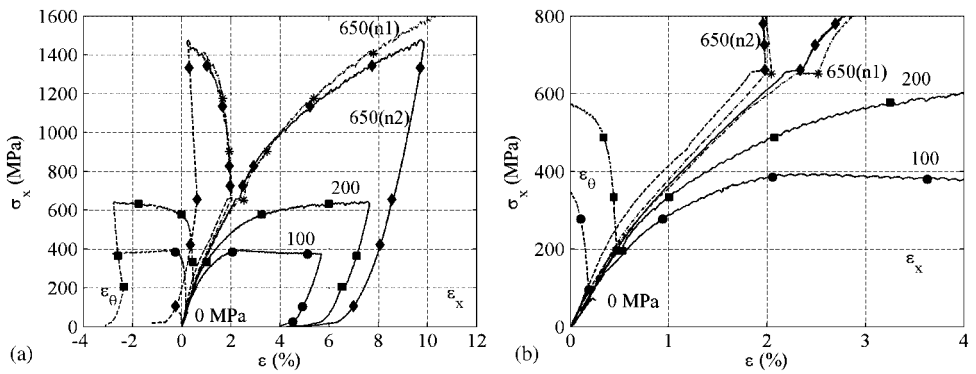

Figure 10. Triaxial tests conducted at different confining pressures p on concrete EC04 (W/C = 0.4): axial stress σ_x vs. strain components ε_x and ε_θ; $p = 0$ MPa (no marker); 100 MPa (circle); 200 MPa (square); 650 MPa (n2) (diamond); 650 MPa (n1) (*, dash-dot line). Zoom on the hydrostatic phases of the loading (figure on the right).

followed by a stiffness reduction, which then becomes constant. The confinement level reached seems too low for concrete stiffening to be perceptible.

Concerning the deviatoric phase of behavior, regardless of the concrete type under consideration, it is shown that the increase in confinement results in a significant increase of both the ductility and loading capacity of the concrete. In addition, for the highest-confinement levels, the positive strain hardening of the material is such that no stress peak can be reached prior to unloading. A comparison of the three concretes reveals that the variation in W/C ratio modifies the confinement threshold, which in turn corresponds to the brittle-ductile transition of the deviatoric behavior. It is obvious, for example, that at a 50 MPa confinement level, concrete EC06 exhibits a softening behavior with a distinct stress peak, while concrete EC08 already presents a behavior of the perfectly plastic type (i.e. a plateau). Similarly, for a 100 MPa confinement level, concrete EC04 offers a stress peak, whereas EC06 and EC08 have a plateau.

DOI: 10.1002/nag

4. VOLUMETRIC BEHAVIOR AND DEVIATORIC BEHAVIOR

In order to more accurately evaluate the effect of W/C ratio on concrete behavior, this section will compare the volumetric behavior and deviatoric behavior curves for the three studied concretes at various confinement levels. The mean stress, volumetric strain and deviatoric stress will all be estimated from the measurements presented in the previous section.

4.1. Tests conducted at 50 MPa confinement

Figure 11 displays the curves of both volumetric behavior (Figure 11(a)) and deviatoric behavior (Figure 11(b)) of concretes EC06 and EC08 tested at a confinement of 50 MPa. The volumetric strain is nearly linear within the hydrostatic phase for the two concretes. It is seen that the volumetric strain of concrete EC08 is greater than that of concrete EC06, particularly during the deviatoric phase of the test. Since the porosity of concrete EC08 is higher than that of EC06, this result had indeed been expected and prove consistent with that obtained from triaxial tests with 15 MPa of confinement on mortars [39].

Figure 11(b) also informs that the maximum deviatoric stress value of concrete EC06 is 13% higher than that of EC08. It can be noted that the difference between unconfined compressive strengths of the two concretes equals roughly 38%. The relative strength variation between the two concretes is thus definitely smaller under the lateral confinement effect.

4.2. Tests conducted at 100 MPa confinement

Figure 12 sets forth the curves of volumetric behavior (Figure 12(a)) and deviatoric behavior (Figure 12(b)) for concretes EC08, EC06 and EC04 tested using 100 MPa of confinement. Figure 12 indicates that the volumetric strain of concrete EC06 is less than that of concrete EC08 yet more than EC04. This expected result may be explained by the porosity deviation between the three concretes. It can also be remarked that the hydrostatic behavior of concrete EC04 remains linear up to 100 MPa, while the other two concretes reveal a sizable reduction in their tangent modulus of compressibility.

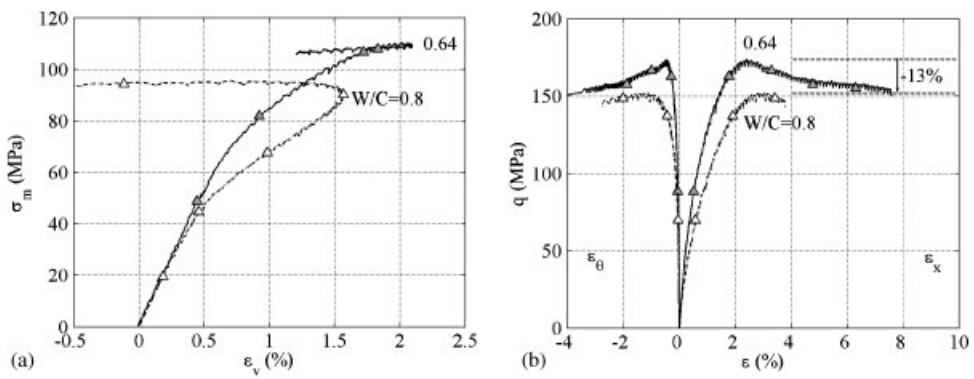

Figure 11. Triaxial tests run at 50 MPa confinement for concretes EC06 (full line with gray symbols) and EC08 (dash-dot line with white symbols): (a) mean stress σ_m vs volumetric strain ε_v and (b) stress deviator q vs strain components ε_x and ε_θ.

DOI: 10.1002/nag

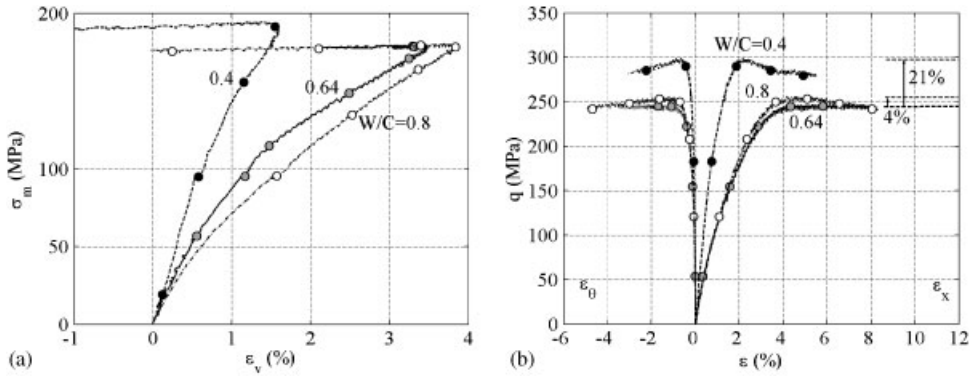

Figure 12. Triaxial tests at 100 MPa confinement for concretes EC04 (dash line with black symbols), EC06 (full line with gray symbols), EC08 (dash-dot line with white symbols): (a) mean stress σ_m vs volumetric strain ε_v and (b) stress deviator q vs strain components ε_x and ε_θ.

The cement matrix of EC04 thus behaves in a near elastic manner for such a confinement level, while the test concretes with higher W/C ratios have already undergone heavy damage.

Figure 12(b) shows that the deviatoric behavior curves of concretes EC08 and EC06 practically overlap with one another. A difference of just 4% exists between the peak stress values for the two concretes, which is insignificant in comparison with the potential dispersion. This result may be explained by the fact that the cement matrix cohesion of these two concretes is strongly damaged during the hydrostatic phase. Upon completion of this phase, the concrete thus behaves almost like a non-cohesive granular stacking. The deviator response of the concrete is highly correlated with its granular stacking and no longer with the cement matrix cohesion.

The studied concretes however have an identical granular skeleton (i.e. identical gravel/sand ratios and aggregate volumes). Only the cement quantity slightly differs between compositions EC06 and EC08 (a deviation of 42 kg/m^3). In assuming that the cement is entirely hydrated, this would correspond to a difference between hydrate volumes that represent less than 3% of the total concrete volume. Granular stacking sequences of concretes EC06 and EC08 are thus very similar, and their weak differences are not perceptible on the concrete deviatoric behavior beyond 100 MPa of confinement.

Figure 12(b) also indicates that the tangent stiffness of concrete EC04 is much higher than the stiffnesses of EC06 and EC08. Moreover, the behavior of concrete EC04 is still of the brittle type and the stress peak value is 21% higher than that of EC06. For this confinement level, the cement matrix of EC04 is still highly cohesive (i.e. displays elastic volumetric behavior), hence, playing an important role in the deviatoric response of this concrete.

4.3. Tests conducted at 200 MPa confinement

Figure 13 presents the curves of volumetric behavior (Figure 13(a)) and deviatoric behavior (Figure 13(b)) of concretes EC06 and EC04 tested at 200 MPa of confinement. Just like at the lower confinement levels, Figure 13(a) highlights that the volumetric strain of concrete EC06 is definitely higher than that of EC04. This effect is easily explained by the porosity difference between the cement matrix of these two concretes.

DOI: 10.1002/nag

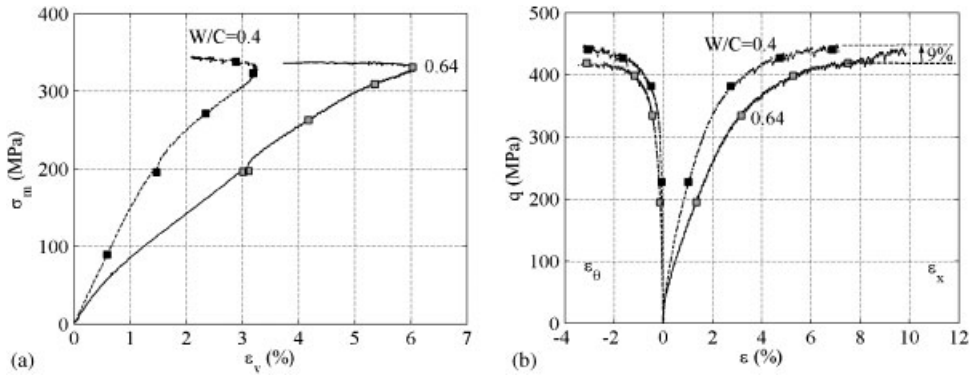

Figure 13. Triaxial tests at 200 MPa confinement for concretes EC04 (dash line with black symbols) and EC06 (full line with gray symbols): (a) mean stress σ_m vs volumetric strain ε_v and (b) stress deviator q vs strain components ε_x and ε_θ.

Figure 13(b) provides evidence that the stiffness of concrete EC04 is higher than that of EC06, yet only slightly so when compared with what had been observed at lower confinement levels. In a similar manner, it is noted that the difference in primary stress value obtained for EC04 is only 9% higher than that of EC06, which remains a small amount in comparison with the deviation observed at 100 MPa confinement. These observations reveal that as confinement increases from 100 to 200 MPa, the cement matrix of concrete EC04 gradually becomes damaged. Furthermore, this damage is highlighted by the non-linearity identified beyond 150 MPa on the hydrostatic behavior (see Figure 13(a)). The deviation in behavior between the two concretes however shows that the cement matrix of EC04 is not completely destroyed and retains significant cohesion under a confining pressure of 200 MPa.

4.4. Tests conducted at 650 MPa confinement

Figure 14 displays the curves of both volumetric behavior (Figure 14(a)) and deviatoric behavior (Figure 14(b)) of concretes EC08, EC06 and EC04 tested in the presence of 650 MPa confinement. It can be observed that the curves obtained for the two samples EC04(n1) and EC04(n2) are very similar, which serves to confirm the low scatter of test results.

A comparison in volumetric behavior of the three concretes described in Figure 14(a) once again shows that the volumetric strain of concrete increases with a rise in W/C ratio. At the quantitative level, it can be noticed that the difference between curves EC06 and EC04 is about twice that observed between curves EC06 and EC08. The difference between porosities of concretes EC06 and EC04 however stands at about twice the difference between porosities of EC06 and EC08. A first-order linear correlation thus exists between concrete porosity variation and the corresponding volumetric strain variation for a given granular skeleton.

Figure 14(a) moreover reveals that beyond 400 MPa of confinement, the volumetric behavior curves of the three concretes seem to run parallel, which suggests that the difference in incremental volumetric strains of the three concretes is significant only at low confinement levels: Typically between 0 and 200 MPa when comparing concretes EC06 and EC08 and between 0 and 400 MPa when comparing EC04 with the other two.

DOI: 10.1002/nag

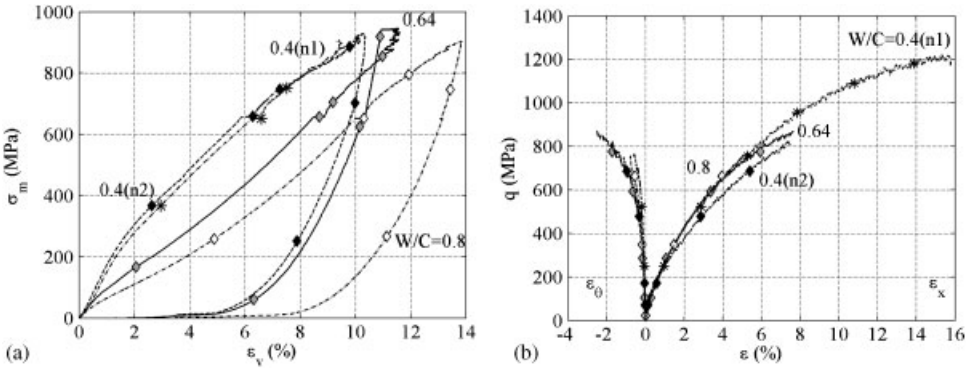

Figure 14. Triaxial tests at 650 MPa confinement for concretes EC06 (full line with gray symbols), EC08 (dash-dot line with white symbols) and EC04 (n2: dash line with black symbols; n1: dash-dot line with asterisk symbols *): (a) mean stress σ_m vs volumetric strain ε_v and (b) stress deviator q vs strain components ε_x and ε_θ.

In addition, Figure 14(b) indicates that the deviatoric behavior curves of concretes EC08, EC06 and EC04 practically overlap. This result confirms that under high confinement, the cement matrix of the concrete loses its cohesion. The concrete behavior is then essentially governed by the granular stacking of the concrete. Since the granular skeleton of the studied concretes is identical, a similar deviatoric behavior for all three studied concretes is to be expected. At first order therefore, under high confinement, concrete behavior becomes insensitive with W/C ratio.

A finer observation of the curves contained in Figure 14(b) nonetheless shows that for deviatoric stress levels above 600 MPa, the (q, ε_x) curves of concrete EC04 samples are slightly stiffer than what was found for EC06. This small difference in behavior may perhaps be explained by the difference between hydrate volumes of the three concretes. If we assume that the concretes have lost their cohesion under such a confinement, the only difference between the three concretes is the difference between hydrates volume (see concrete composition Table I). This difference is equal to 7% of the concrete volume if we compare EC04 and EC06 composition, whereas it is 3% between EC06 and EC08. If this difference is small in regards of the concrete composition, it still exists. The beginning of the deviatoric phase of the tests incites a rearrangement of the grains within the concrete, which is characterized at the macroscopic level by an increase in volumetric strain in comparison with a hydrostatic test using the equivalent mean stress (i.e. deviatoric phase of Figure 14(a)). It can thus be assumed that at low deviatoric stress levels, the small difference in fines volume stemming from hydrate destruction does not play any significant role in the granular stacking behavior. On the other hand, for higher levels, as the material density increases and porosity very strongly decreases, it is plausible that the difference in fines volume between the three concretes becomes perceptible.

5. LIMIT STATES

During the experimental characterization of material behavior, various criteria may be used to identify the material's limit–state curve. The most commonly used criterion is defined as the

DOI: 10.1002/nag

stress state associated with the maximum deviatoric stress that the material can support (i.e. the stress limit state). For geomaterials exhibiting a dilating behavior on fracture, this stress limit state often lies close to the stress state associated with the transition point from material contraction to dilatancy. This state corresponds to the maximum volumetric strain state in terms of the material's potential contraction. For the following discussion, we will define this stress state as a strain limit state of the concrete.

The test results presented in Sections 3 and 4 indicate that for samples tested at a high confinement level, the experimental device employed is no longer able to achieve the maximum stress value before test unloading. It is no longer possible therefore to characterize the stress limit state of the concrete for high confinement levels. Only the strain limit state can be identified for all of the tested samples. This transition has been estimated from the volumetric behavior curves of the tested samples (see Figures 7(b), 11(a), 12(a), 13(a), 4(a)). These figures show that at low confinements, since the concrete exhibits a brittle response, the strain limit state practically coincides with the stress limit state of the concrete. The strain limit state has thus been chosen as the reference state for purposes of this study.

Figure 15(a) summarizes the strain limit state of concretes EC08, EC06 and EC04 within the (σ_m, q) deviatoric plane for all tests performed. It can be observed that the loading capacity of concrete strongly increases in a quasi-linear manner with respect to the mean stress increase.

Figure 15(b) sets forth the same limit states in a $(\sigma_m, q/q_{EC06})$ plane, where q_{EC06} is the limit deviator obtained for reference concrete EC06 at an identical confining pressure. This presentation in terms of deviator relative to that of the reference concrete provides a better perception of the differences between the three concretes. This figure makes it possible to verify that for low mean stress levels, the limit state of the concrete is heavily dependent on W/C ratio, i.e. on cement matrix strength. This result was obviously the expected one. In contrast, the same figure also shows that this dependence of concrete limit state on W/C ratio decreases rapidly as mean stress rises. Beyond a critical mean stress σ_{mc}, the limit state curve actually becomes independent of W/C ratio.

This critical mean stress is itself dependent upon W/C ratio and increases as the W/C ratio drops, which indicates that the mean stress level beyond which the W/C ratio no longer exerts any influence is even greater when the cement matrix strength is high. In reading Figure 15(b), as W/C decreases from 0.64 to 0.4, σ_{mc} increases from 180 to 330 MPa.

Interpretation of the above results may proceed as follows. At a low-level mean stress ($\sigma_m \ll \sigma_{mc}$), the concrete behavior is to a large extent governed by cement matrix cohesion. The contraction-dilatancy transition is associated with the opening of microcracks within the material structure during gradual damage of the cement matrix [45]. For a given mean stress level, as the W/C ratio of the concrete drops, both cement matrix cohesion and concrete strength increase.

As the mean stress level increases ($\sigma_m \approx \sigma_{mc}$), the relative difference between residual cohesion of the various concretes narrows, leading to a reduction in deviations between the reached deviatoric stresses. At a high mean stress level ($\sigma_m > \sigma_{mc}$), the cement matrix cohesion of the concrete is completely destroyed, with the concrete then behaving like a granular stacking. The strain limit state of the concrete corresponds to the maximum compactness that this stacking can achieve. The granular skeletons of the studied concretes are all identical and the associated stacking sequences very close to one another. Beyond the critical mean stress therefore, the three concretes all behave identically regardless of their W/C ratio.

The failure surface of concrete has been described in various ways for numerical modeling purpose. In most common models, one can find three kinds of meridian cross section of the failure

DOI: 10.1002/nag

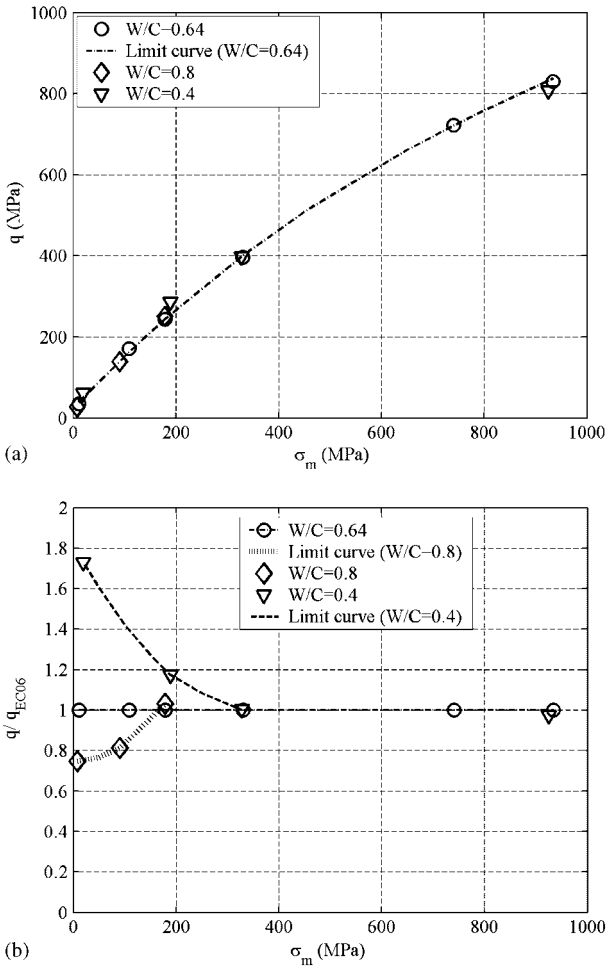

Figure 15. Limit states of concretes EC04, EC06 and EC08: (a) deviatoric stress q vs mean stress σ_m and (b) relative deviator q/q_{EC06} vs mean stress σ_m, where q_{EC06} is the deviatoric stress associated with the limit state of reference concrete EC06.

surface: linear [46, 47], parabolic [48–51] or power law [52]. To compare these models with the results, a comparison between the limit states of the EC06 concrete and these three kinds of failure surfaces is shown in a log–log plot in Figure 16(a). The best fitting parameters and the discrepancy with the measurements are displayed in Table IV. For mean stresses higher than 100 MPa, the limit state curve is almost linear and the three kinds of model are close to the results. However, the power law gives the best fitting with a mean error equal to 3%. For lower mean stresses the linear or parabolic criterions lead to an overestimation of the concrete strength. These criterions are not able to fit the unconfined compression strength whereas the power law is close to measurements in the all range. One can notice that the identified exponent of the power law ($c=0.758$) is very

DOI: 10.1002/nag

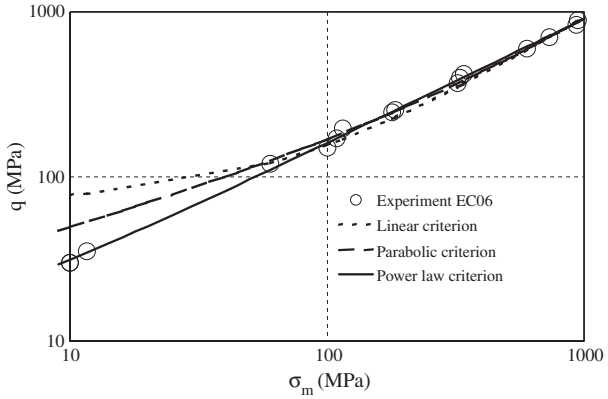

Figure 16. Comparison between the limit states of the EC06 concrete ant the most common concrete criterions; experiment EC06 (o); linear criterion $q=b+c\sigma_m$ (dot line); parabolic criterion $q=(a+b\sigma_m+c\sigma_m^2)^{1/2}$ (dash line); power law criterion $q=a(b+\sigma_m)^c$ (full line).

Table IV. Identified parameters from common criterion and discrepancy between the measurements and the fittings.

	Linear $q=b+c\sigma_m$	Parabolic $q=(a+b\sigma_m+c\sigma_m^2)^{1/2}$	Power law $q=a(b+\sigma_m)^c$
a (MPa^{α})	—	177	4.81
b (MPa)	68.7	221	1.82
c	0.868	0.621	0.758
mean error (%)	32	14	3
mean error*(%)	6	4	3
max error*(%)	14	12	9

*Error calculated without taking into account the unconfined compression tests.

close to the one proposed by Kang ($c=0.77$, [52]) from various experimental results taken from the literature.

Let us assume that a power law criterion is also valid for the EC04 and EC08 concretes:

$$q=a(b+\sigma_m)^c \tag{3}$$

Since their respective failure surfaces lead to the same one as σ_m increases, that means that a and c have to be the same than the one identified for the EC06 concrete. These coefficients would be then only dependent on the aggregates, whereas b would be characteristic of the cement paste strength. Figure 17 shows that such an assumption is in agreement with the experiments. We can observe that the limit states of the three concretes are very close from the power law criterion, using the coefficients previously identified ($a=4.81$ and $c=0.758$, see Table IV). In this figure, only the coefficient b has been chosen for the concrete EC04 and EC08, to reproduce the experiments in the best possible way ($b_{EC04}=8\,\text{MPa}$; $b_{EC08}=0.4\,\text{MPa}$).

DOI: 10.1002/nag

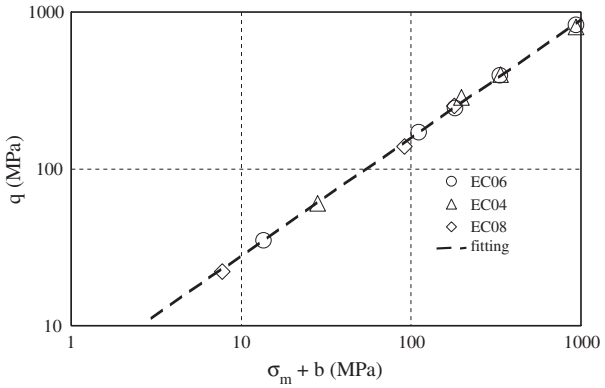

Figure 17. Limit states of concretes EC04, EC06 and EC08: log(q) vs $\log(\sigma_m + b)$; EC06 $b = 1.82$ MPa (o); EC04 $b = 8$ MPa(Δ); EC08 $b = 0.4$ MPa ($\diamond$); power law fitting $q = a(b + \sigma_m)^c$ where $a = 4.81\,\mathrm{MPa}^{1-c}$ and $c = 0.758$ (dash line).

6. CONCLUSION

The context of this study has focused on identifying concrete behavior under severe triaxial loadings. In order to reproduce high stress levels with well-controlled loading paths, static tests were carried out on concrete samples through the use of a very high-capacity triaxial press. The test results presented in this article relate more specifically to the effect of W/C ratio, entering into the concrete composition, on concrete behavior under high confinement. Based on an ordinary reference concrete (W/C = 0.6), two other concretes with W/C ratios equal to 0.4 and 0.8, respectively, were produced. Triaxial test results have yielded the following conclusions.

During the deviatoric phase of behavior, regardless of the W/C ratio of concrete, it can be determined that the confinement very sharply raises both the ductility and the loading capacity of the concrete. A comparison of the three tested concretes found that a drop in W/C ratio pushes the confinement threshold higher, which corresponds to the brittle-ductile behavior transition.

The volumetric behavior curves of concrete show that compaction increases with the W/C ratio, and in particular at low confinement levels. A first-order linear correlation thus exists between porosity variation of a concrete and its volumetric strain variation for a given granular skeleton.

Conversely, under high confinement, once the cement matrix has been strongly damaged, the volumetric behavior and deviatoric behavior of the concrete both become insensitive to W/C ratio.

Lastly, the comparison of limit-states for the three concretes reveals, as could have been expected, that for low mean stress levels, the limit state of the concrete depends very strongly on W/C ratio. This dependence of concrete limit state on W/C ratio however falls rapidly as mean stress increases. Beyond a critical mean stress, the limit state curve becomes independent of W/C ratio. For lower W/C ratios of the concrete, this critical mean stress reach higher values and proves even greater when the cement matrix is strong.

In summary, the test results provided in this article show that under high confinement, the concrete behaves like a non-cohesive granular stacking, on which the cement matrix strength of the fresh concrete no longer exerts any influence. From an application standpoint, these results highlight

DOI: 10.1002/nag

the very small advantages to be gained by increasing the cement concentration in concretes for the purpose of raising their strength capacity to resist extreme loadings.

ACKNOWLEDGEMENTS

The GIGA press has been installed in the 3S-R laboratory within the framework of a cooperative agreement with the Délégation Générale pour l'Armement (CEG, DGA, French Ministry of Defense). This research has been performed with the financial support of the 'Centre d'Etudes de Gramat' (CEG, DGA).

REFERENCES

1. Zukas JA. *Penetration and Perforation of Solids*, *Impact Dynamics*. Krieger Publishing Company: New York, 1992.
2. Bailly P, Tombini C, Le Vu O. Modélisation de géomatériaux sous sollicitations dynamiques élevées. I: un tir de pénétration sur cible en béton. *Colloque du Réseau GEO*, Aussois, France, 2–6 Décembre 1996 [in French].
3. Li H, Pugh D. *Mechanical Behavior of Materials Under Pressure*. Elsevier: Amsterdam, 1970.
4. Kupfer HB, Gerstle KH. Behavior of concrete under biaxial stresses. *Journal of the Engineering Mechanics*, *Division* 1973; **99**(4):853–866.
5. Wang C-Z, Guo Z-H, Zhang X-Q. Experimental investigation of biaxial and triaxial compressive concrete strength. *ACI Materials Journal* 1987; **84**:92–100.
6. Jiang LH, Huang DH, Xie NX. Behavior of concrete under triaxial compressive–compressive–tensile stresses. *ACI Materials Journal* 1991; **88**(2):181–185.
7. Imran I, Pantazopoulou SJ. Experimental study of plain concrete under triaxial stress. *ACI Materials Journal* 1996; **93**(6):589–601.
8. Taliercio A, Berra M, Pandolfi A. Effect of high-intensity sustained triaxial stresses on the mechanical properties of plain concrete. *Magazine of Concrete Research* 1999; **51**(6):437–447.
9. Sfer D, Carol I, Gettu R, Etse G. Study of the behavior of concrete under triaxial compression. *Journal of Engineering Mechanics* 2002; **128**(2):156–163.
10. Hopkinson B. A method of measuring the pressure in the deformation of high explosives or by the impact of bullets. *Philosophic Transactions of the Royal Society* 1914; **A213**:437–452.
11. Zhao H, Gary G. On the use of SHPB techniques to determine the dynamic behavior of materials in the range of small strains. *International Journal of Solids and Structures* 1996; **33**(23):3363–3375.
12. Bischoff PH, Perry SH. Compressive behaviour of concrete at high strain rates. *Materials and Structures* 1991; **24**:425–450.
13. Toutlemonde F. Résistance au choc des structures en béton: du comportement du matériau au calcul des ouvrages. *Ph.D. Thesis of Ecole Nationale des Ponts et Chaussées*, 1995 [in French].
14. Hild F, Denoual C, Forquin P, Brajer X. On the probabilistic–deterministic transition involved in a fragmentation process of brittle materials strains. *Computers and Structures* 2003; **81**(12):1241–1254.
15. Rossi P, Van Mier JGM, Toutlemonde F, Le Maou F, Boulay C. Effect of loading rate on the strength of concrete subjected to uniaxial tension. *Materials and Structures* 1994; **27**(5):260–264.
16. Schmidt JM. High pressure and high strain rate behaviour of cementitious materials: experiments and elastic/viscoplastic modeling. *Ph.D. Thesis*, University of Florida, U.S.A., 2003.
17. Bazant ZP, Bishop FC, Chang TP. Confined compression tests of cement paste and concrete up to 300 Ksi. *ACI Journal* 1986; **33**:553–560.
18. Buzaud E. Performances mécaniques et balistiques du microbéton MB50. *The Scientific Report Comportement des ouvrages en Dynamique Rapide*, comportement dynamique du béton, project leader P. Bailly, 1998 [in French].
19. Burlion N, Pijaudier-Cabot G, Dahan N. Experimental analysis of compaction of concrete and motar. *International Journal for Numerical and Analytical Methods in Geomechanics* 2001; **25**:1467–1486.
20. William EM, Akers SE, Reed PA. Constitutive models for the triaxial behaviour of concrete. *Report No. ERDC/GSL TR-05-16*, Geotechnical and Structures Laboratory, U.S. Army, 2005.
21. Akers SA, Phillips BR. Concrete modelled as un inhomogeneous material: numerical simulations of contact detonation charges. *18th International Symposium on the Military Aspects of Blast and Shock*, Oberjettenberg, Germany, September 2004.

DOI: 10.1002/nag

22. Schmidt JM, Cazacu O, Green ML. Experimental and theoretical investigation of the high-pressure behavior of concrete. *International Journal for Numerical and Analytical Methods in Geomechanics* 2008; DOI: 10.1002/nag.700.
23. Warren T, Fossum A, Frew D. Experimental investigation of size effect in concrete fracture under multiaxial compression into low-strength (23 MPa) concrete: target characterization and simulations. *International Journal of Impact Engineering* 2004; **30**:477–503.
24. Gabet T, Malécot Y, Daudeville L. Triaxial behavior of concrete under high stresses: influence of the loading path on compaction and limit states. *Cement and Concrete Research* 2008; **38**(3):403–412.
25. Poinard C, Malecot Y, Daudeville L. Damage of concrete in a very high stress state: experimental investigation. *Materials and Structures* 2009; DOI: 10.1617/s11527-008-9467-6.
26. Dupray F, Malecot Y, Daudeville L, Buzaud E. A mesoscopic model for the behaviour of concrete under high confinement. *International Journal for Numerical and Analytical Methods in Geomechanics* 2009; DOI: 10.1002/nag.771.
27. Vu XH, Malecot Y, Buzaud E, Daudeville L. Experimental analysis of concrete behavior under high confinement: effect of the saturation ratio. *International Journal of Solids and Structures* 2009; **46**:1105–1120. DOI: 10.1016/j.ijsolstr.2008.10.015.
28. Féret R. Sur la compacité des mortiers hydrauliques. *Annales des Ponts et Chaussées*, *Série 7* 1892; **4**:5–164 [in French].
29. Bolomey J. Granulation et prévision de la résistance probable des bétons. *Travaux* 1935; **19**(30):228–232 [in French].
30. Neville AM. *High Alumina Cement Concrete*. John Wiley & Sons, Inc.: New York, 1975; 201.
31. Gilkey HJ. Water/cement ratio versus strength—another look. *Journal of the American Concrete Institute*, *Part 2* 1961; **58**:1951–1978.
32. Alexander KM, Ivanusec I. Long term effects of cement SO_3 content on the properties of normal and high-strength concrete, part I. The effect on strength. *Cement and Concrete Research* 1982; **12**(1):51–60.
33. Kakizaki M, Edahiro H, Tochigi T, Niki T. Effect of mixing method on mechanical properties and pore structure of ultra high-strength concrete. *Katri Report No. 90*, 1992; 19.
34. Roy DM, Gouda GR. Porosity–strength relation in cementitious materials with very high strengths. *Journal of the American Ceramic Society* 1973; **53**(10):549–550.
35. Sersale R, Cioffi R, Frigione G, Zenone F. Relationship between gypsum content, porosity, and strength of cement. *Cement and Concrete Research* 1991; **21**(1):120–126.
36. Chanvillard G. Le matériau béton: connaissances générales. Aléas, 1999; 115–139 [in French].
37. Ollivier JP, Buil M. Conception des bétons: la structure poreuse, La durabilité des bétons, *Presses de l'ENPC*, Eds., Paris, 1992 [in French].
38. Burlion N. Compaction des bétons: éléments de modélisation et caractérisation expérimentale. *Ph.D. Thesis of Ecole Normale Supérieure de Cachan*, France, 1997 [in French].
39. Yurtdas I, Peng H, Burlion N, Skoczylas F. Influence of water by cement ratio on mechanical properties of mortars submitted of drying. *Cement and Concrete Research* 2006; **36**(7):1286–1293.
40. Ingénierie T. *la Croix Blanche*, 46130 Saint Michel Loubejou, France (Thiot 2004).
41. Vu XH. Caractérisation expérimentale du béton sous fort confinement: influences du degré de saturation et du rapport eau/ciment. *Ph.D. Thesis of Université Grenoble I*, 2007 [in French].
42. Gabet T, Vu XH, Malécot Y, Daudeville L. A new experimental technique for the analysis of concrete under high triaxial loading. *Journal de Physique IV* 2006; **134**:635–640.
43. ACI 363R-92. State-of-the-art report on high-strength concrete. *ACI Manual of Concrete Pratice*, *Part 1*: *Materials and General Properties of Concrete*, Detroit, MI, 1994; 55.
44. ACI 318-89. Building code requirements for structural concrete. *ACI Manual of Concrete Pratice*, *Part 3*: *Use of Concrete in Buildings—Design*, *Specifications and Related Topics*, Detroit, MI, 1996; 345.
45. Mazars J. Application de la mécanique de l'endommagement au comportement non-linéaire et à la rupture du béton de structure. *Ph.D. Thesis of Université Paris VI*, France, 1984 [in French].
46. Drucker DC, Prager W. Soil mechanics and plastic analysis on limit design. *Quarterly of Applied Mathematics* 1952; **10**(2):157–165.
47. Williams KJ, Warnke EP. Constitutive model for the triaxial behaviour of concrete. *International Association of Bridge and Structural Engineers Seminar on Concrete Structures Subjected to Triaxial Stresses*, *Paper III-1*, Bergamo, 1974.
48. Schleicher F. Der Spannungszustand an der Fliessgrenze (Plastizitätsbedingung). *Zeitschrift für angewandte Mathematik und Mechanik* 1926; **6**:199–216. 45 [in Germany].

49. Nadai A. *Theory of Flow and Fracture of Solids*, vol. 1. McGraw-Hill: New York, 1950.
50. Krieg R. A simple constitutive description for soils and crushable foams. *Report SC-DR-72-0883*, vol. 46. Sandia National Laboratories: Albuquerque, 1972; 94–168.
51. Swenson DV, Taylor LM. A finite element model for the analysis of tailored pulse simulation of boreholes. *International Journal for Numerical and Analytical Methods in Geomechanics* 1983; **7**(4):469–484.
52. Kang HD, Willam K. Localization characteristics of triaxial concrete model. *Journal of Engineering Mechanics* (ASCE) 1999; **125**:941–950.

DOI: 10.1002/nag